PASJ: Publ. Astron. Soc. Japan **48**, 211–218 (1996)

The Variable O VIII Warm Absorber in MCG−6–30–15

Chiko OTANI,[1] Tsuneo KII,[2] Christopher S. REYNOLDS,[3] Andrew C. FABIAN,[3]
Kazushi IWASAWA,[3,4] Kiyoshi HAYASHIDA,[5] Hajime INOUE,[2] Hideyo KUNIEDA,[4]
Fumiyoshi MAKINO,[2] Masaru MATSUOKA,[1] and Yasuo TANAKA[6]

[1] *The Institute of Physical and Chemical Research (RIKEN), Hirosawa, Wako, Saitama 351-01*
E-mail (CO) otani@postman.riken.go.jp
[2] *The Institute of the Space and Astronautical Science, Yoshinodai, Sagamihara, Kanagawa 229*
[3] *Institute of Astronomy, Madingley Road, Cambridge CB3 OHA, UK*
[4] *Department of Astrophysics, Nagoya University, Furo-cho, Chikusa-ku, Nagoya 464-01*
[5] *Department of Earth and Space Science, Osaka University, Machikaneyama, Toyonaka, Osaka 560*
[6] *Max-Planck-Institut für Extraterrestrische Physik, Giessenbachstrasse, D-85740 Garching, Germany*

(Received 1995 November 16; accepted 1996 January 22)

Abstract

We present the results of a 4-day ASCA observation of the Seyfert galaxy MCG−6–30–15, focusing on the nature of X-ray absorption by the warm absorber, characterized by the K-edges of highly ionized oxygen, O VII and O VIII. We have confirmed that the column density of O VIII changes on a timescale of $\sim 10^4$ s when the X-ray continuum flux decreases. A significant anti-correlation of the column density with the continuum flux gives direct evidence that the warm absorber is photoionized by the X-ray continuum. From the timescale of the variation of the O VIII column density, we have estimated that it originates from gas within a radius of about 10^{17} cm of the central engine. In contrast, the depth of the O VII edge shows no response to the continuum flux, which indicates that it originates in gas at larger radii. Our results strongly suggest that there are two warm absorbing regions: one is located near or within the Broad Line Region; the other is associated with the outer molecular torus, scattering medium or Narrow Line Region.

Key words: Galaxies: individual (MCG−6–30–15) — Galaxies: Seyfert — Galaxies: X-rays

1. Introduction

Soft X-ray observations of many Seyfert 1 galaxies have now shown evidence for an absorption edge due to partially-ionized oxygen along the line of sight to the active nucleus (Nandra, Pounds 1992; Nandra et al. 1993; Fabian et al. 1994; Mihara et al. 1994). Since the absorbing medium is plausibly at about 10^5 K, it is known as the warm absorber. Its high occurrence indicates that the fraction of the nucleus covered by this material is high, perhaps 50%, which, combined with a typical column density of $\sim 10^{22}$ cm^{-2}, suggests that it is an important constituent of the region surrounding the nucleus. The product of the covering fraction and column density are at least as large as that for the clouds responsible for the optical/UV broad line emission.

The location of the warm absorber has been unclear. If it is assumed that it is in photoionization equilibrium, it must lie within about 30 pc of the nucleus. This value is deduced from the ionization parameter, $\xi = L/(nR^2) \approx 30\,\mathrm{erg\,cm\,s^{-1}}$, obtained from fits to the data in MCG−6–30–15 (Fabian et al. 1994), where L is the X-ray luminosity ($\sim 10^{43}\,\mathrm{erg\,s^{-1}}$), and the product ($nR$) is the maximum column density ($\sim 10^{22}\,\mathrm{cm^{-2}}$).

Further progress can be made from considerations of the variability of the warm absorber. ASCA data from 1993 show that the warm absorber in MCG−6–30–15 varies on timescales of a few hours (Reynolds et al. 1995). This provides a lower limit on the recombination timescale of the gas, and thus an upper limit on the radius, which was less than $\sim 10^{17}$ cm. However, the situation based on those data was confusing, since it appeared that the ionization parameter did not scale simply and linearly with the ionizing luminosity, as would be expected from the nature of that parameter, but that it varied in some more complex manner.

Here, we report on the results from a 4-day ASCA observation of MCG−6–30–15 taken in 1994. The warm absorber changed during the last day, giving a deeper feature as the flux diminished. We have shown that this and previous observations can now be understood if there are *two* warm absorbers, instead of one. The outer one dominates the O VII edge and has a long recombination time, so the O VII edge does not change; the inner one

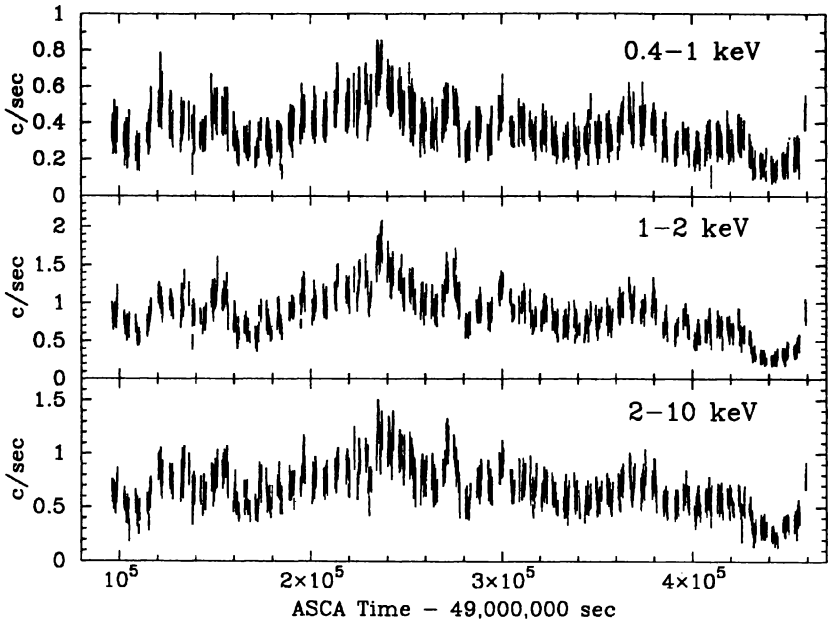

Fig. 1. SIS light curve of MCG−6−30−15 in three bands (0.4–1 keV, 1–2 keV, and 2–10 keV). The horizontal axis is given in seconds from ASCA time = 49 000 000 s = 03 : 06 : 38 22 1994 July (UT). The vertical axis is in units of count rate per SIS. Each bin width is typically 100 s. No background subtraction is applied because it is negligible.

dominates the O VIII edge and has a recombination time of 10^4 s or less, so the O VIII edge responds directly to the ionizing radiation.

The inner warm absorber is very thin, suggesting that it consists of many clouds. There may then be problems with the stability of the clouds, which presumably are pressure-confined in some way, since there is only a narrow range of parameter space in which the necessary clouds can exist if the confining pressure is the thermal pressure of a hotter, more tenuous, medium also in photoionization equilibrium with the ionizing radiation (Reynolds, Fabian 1995). We explore the constraints imposed by these clouds and note that the inner warm absorber must contain a considerable reservoir of gas in which oxygen is completely ionized in order to provide O VIII when the ionizing flux drops.

2. Observation and Results

2.1. Mean Spectrum

MCG−6−30−15 was observed with ASCA during 1994 July 23–27. Both Solid-state Imaging Spectrometers, SIS-0(S0) and SIS-1(S1), were operated in 1-CCD Faint mode, and both Gas Imaging Spectrometers, GIS-2(G2) and GIS-3(G3), were in normal PH mode. Since the GIS does not have the energy range to investigate the oxygen absorption edge features well, we concentrate here on only the SIS data.

All of the data used were selected from intervals of high and medium bit rates. The SIS data were selected using the following local criteria: a) the times were more than 3 min from the SIS Radiation Belt Monitor flag being triggered by the South Atlantic Anomaly (SAA), b) the angle between the field of view and the edge of the bright and dark earth exceeded 25° and 5°, respectively, and c) the cutoff rigidity was greater than 4 GeV c^{-1}. After these selections, we also deleted data if d) the background rate was abnormally high near the SAA, e) there were any spurious events, and f) the dark frame error was abnormal. The net exposure time was about 166 ks in each SIS. The source varied during our observation by a factor ~ 7 (figure 1).

Fitting the mean spectrum by a simple power-law model with a power-law model clearly shows the presence of edge-like absorption features between 0.7 and 2 keV, a complex excess around 5–7 keV, and a further excess at 0.6 keV. The 0.7–2 keV feature is similar to that reported by Fabian et al. (1994). The line feature around 5–7 keV is probably due to reflection from the relativistic inner accretion disk, as discussed by Tanaka et al. (1995).

In order to estimate the properties of the feature below 1 keV, we now restrict the energy range of our analysis to below 4 keV, because of the iron line feature above

Table 1. Spectral fittings of the 0.4–5 keV mean spectrum.

Model	Photon index Γ	$N_{\rm H}$ ($10^{20}\,{\rm cm}^{-2}$)	$E_{\rm edge}$ (keV)	$\tau_{\rm edge}$	$E_{\rm line}$* (keV)	EW (eV)	χ^2/ν
PL & 2 edges	$1.840^{+0.007}_{-0.008}$	...	$0.720^{+0.005}_{-0.005}$ $0.851^{+0.013}_{-0.013}$	$0.58^{+0.04}_{-0.04}$ $0.20^{+0.03}_{-0.07}$	...	...	994.6/513
PL & 2 edges & 0.6 keV line	$1.92^{+0.008}_{-0.009}$	...	$0.721^{+0.004}_{-0.005}$ $0.849^{+0.015}_{-0.014}$	$0.55^{+0.04}_{-0.04}$ $0.19^{+0.03}_{-0.03}$	$0.61^{+0.01}_{-0.01}$	14^{+3}_{-3}	905.2/511
PL & 2 edges absorption	$1.93^{+0.02}_{-0.02}$	$2.0^{+0.4}_{-0.4}$	$0.720^{+0.004}_{-0.004}$ $0.864^{+0.013}_{-0.012}$	$0.63^{+0.04}_{-0.04}$ $0.25^{+0.03}_{-0.04}$	...	...	896.4/512
PL & 2 edges & line & absorption	$1.92^{+0.02}_{-0.02}$	$2.3^{+0.4}_{-0.4}$	$0.721^{+0.005}_{-0.005}$ $0.863^{+0.014}_{-0.012}$	$0.60^{+0.04}_{-0.03}$ $0.24^{+0.03}_{-0.03}$	$0.60^{+0.01}_{-0.01}$	17^{+3}_{-4}	780.3/510

* Line width is fixed to zero. Line energy is not corrected for redshift.

5 keV. At least two absorption edges are needed to explain the broad trough around 0.7–1 keV. In addition, we included the excess neutral absorption above the Galactic hydrogen column density ($N_{\rm H} = 4.06 \times 10^{20}\,{\rm cm}^{-2}$; Elvis et al. 1989) and a Gaussian line at 0.6 keV to suppress the hollow at 0.5 keV and the excess at 0.6 keV. It is plausible that these features are of instrumental origin, because the change in the spectral slope, as seen below, may cause such a feature near these energies where the response function has a sharp feature. In addition, the response matrix for these energies still includes some uncertainties due to the absence of a good calibrator for SIS. The final fitting results are shown in table 1. (The errors indicate the 90% confidence levels for two interesting parameters.) The fluctuation of the derived parameters for the absorption edges are almost consistent with each other, which means that the inclusions of the neutral absorption and a 0.6 keV line do not change our results on the edge parameters. The absorption-edge model is only affected by the local structure at and above the edge threshold energy.

The rest-frame threshold energy of the lower edge has been determined to be 0.721 ± 0.005 keV, which is near, but slightly lower than, that of the O VII edge. This tendency is almost unchanged by the models used, and is also seen in the fitting results of the spectra divided in time, as shown below. Although the threshold energy of the higher energy edge depends slightly on the model, its range is consistent with the O VIII edge energy, 0.871 keV. (Although the energies are similar to those of the neutral iron L and neon K edges, the required high abundances of these elements, and the lack of iron M and neon L absorption, indicate that this is a mere coincidence.) We conclude that the observed absorption feature is dominated by O VII and O VIII edges, as shown by Fabian et al. (1994). We emphasize that the small energy shift is greater in O VII than in O VIII. The hydrogen-equivalent column densities of the observed O VII and O VIII are $N_{\rm H}$(O VII)= $(3.0^{+0.2}_{-0.2}) \times 10^{21}\,{\rm cm}^{-2}$ and $N_{\rm H}$(O VIII)= $(2.8^{+0.4}_{-1.0}) \times 10^{21}\,{\rm cm}^{-2}$, respectively, assuming the cosmic abundance for the absorbing matter. The mean column density is consistent with that in the first observation of Fabian et al. (1994).

We also tried a simple warm absorber model, as described in Fabian et al. (1994), allowing the photon index to vary. The obtained parameters are $\xi = 17^{+2}_{-2}\,{\rm erg\,cm\,s}^{-1}$ and $N_{\rm H} = (4.6^{+0.3}_{-0.2}) \times 10^{21}\,{\rm cm}^{-2}$ when the extra neutral absorption and the 0.6 keV line are included. The model is worse than the two-edge model due mainly to the energy shift of the O VII edge. We mainly use the two-edge model below.

2.2. *Time Variability of the Warm Absorber*

In order to follow a change in the low-energy absorption features, we divided the whole 4-day observation into 17 parts, each of which has about a 10 ks integration time. The background for each spectrum was subtracted using the spectrum obtained in off-source regions from the same CCD chip and during the same time interval. (Note that the background subtraction had little effect on our results.) The observation log for these divisions is given in table 2. We fit the spectra using a model containing a power-law continuum, two edges, and neutral absorption above the Galactic value. The results are listed in table 3 and are shown in figure 2.

The depth of the O VII absorption edge is consistent with being constant during our observation with $\chi^2_\nu = 1.20$ for $\nu = 16$ in the constant hypothesis. (Here, we used 1σ errors for one interesting parameter.) However, a significant increase in the O VIII depth with a decrease

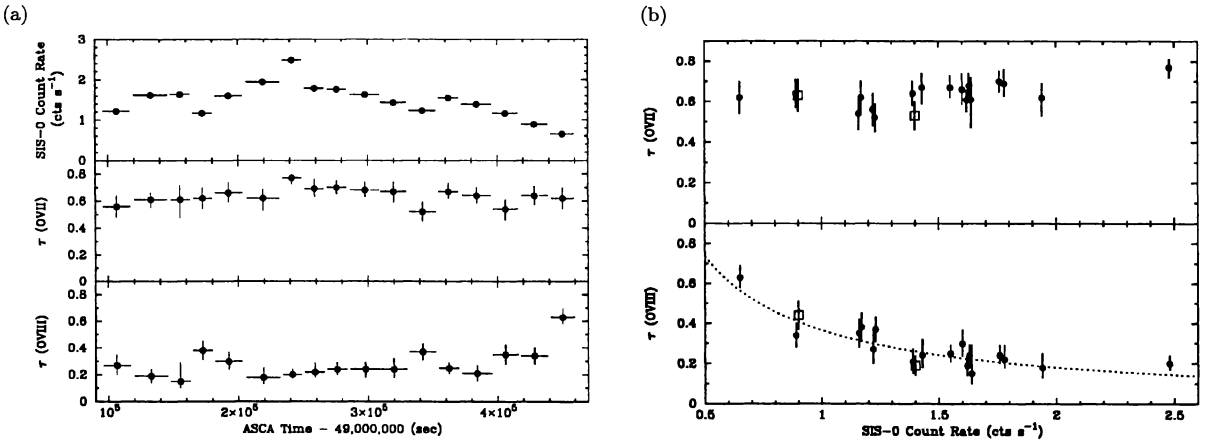

Fig. 2. Time variability of the absorption edge features. (a) Light-curves of the continuum flux in count rate in 0.4–10 keV and depths of the O VII and O VIII absorption edges. The typical duration of each point is 20 000 s. (b) Flux dependence of the absorption depths of O VII and O VIII edges (filled circle). The data points by Reynolds et al. (1995) are also plotted (square). The curve expressed by equation (1) is plotted by dots in the lower panel (see text). The vertical error bars correspond to 1σ for one interesting parameter.

Table 2. Log for the divided spectra.

No.	Epoch start	Epoch end	Exposure (s)	Flux (c s^{-1} SIS^{-1})
1.....	7/23 05:49	7/23 11:30	10500	1.22
2.....	7/23 12:28	7/23 19:30	9500	1.62
3.....	7/23 20:11	7/24 00:18	9500	1.64
4.....	7/24 00:59	7/24 05:05	8000	1.17
5.....	7/24 05:46	7/24 11:29	10500	1.60
6.....	7/24 12:28	7/24 19:28	10300	1.94
7.....	7/24 20:09	7/25 00:16	9300	2.48
8.....	7/25 00:57	7/25 05:04	9100	1.78
9.....	7/25 05:44	7/25 09:51	9000	1.76
10.....	7/25 10:43	7/25 16:59	9300	1.63
11.....	7/25 17:17	7/25 22:39	10600	1.43
12.....	7/25 23:19	7/26 05:02	9700	1.23
13.....	7/26 05:42	7/26 09:50	9200	1.55
14.....	7/26 10:40	7/26 16:56	9800	1.39
15.....	7/26 17:12	7/26 22:38	11400	1.16
16.....	7/26 23:17	7/27 05:01	10400	0.89
17.....	7/27 05:41	7/27 10:43	9800	0.65

in the incident continuum flux was clearly detected at the end of the observation. (See the comparison of the spectra in epochs 14 and 17 in figure 3.) Statistically, the hypothesis of a constant O VIII depth in epochs 1–17 gives $\chi^2_\nu = 3.41$ for $\nu = 16$, and it is rejected with more than a 99% confidence level. This χ^2_ν value relies mainly on the great depth in epoch 17, which is above 6σ from the mean, $\tau_{\rm O\,VIII} = 0.27 \pm 0.02$, in epochs 1–16. On the other hand, the depths in epochs 1–16 are consistent with this mean within 1.6 σ.

These tendencies of both edges are quantitatively consistent with those observed in the PV phase spectra (Fabian et al. 1994; Reynolds et al. 1995), in which the optical depths of O VII and O VIII were $\tau_{\rm O\,VII} = 0.53 \pm 0.07$ and $\tau_{\rm O\,VIII} = 0.19 \pm 0.05$ in the observation on 1993 July 8–9 (the count rate was 1.4 ct s^{-1} in SIS-0), and $\tau_{\rm O\,VII} = 0.63 \pm 0.08$ and $\tau_{\rm O\,VIII} = 0.44 \pm 0.07$ in the observation on 1993 July 31–August 1 (the count rate was then 0.9 ct s^{-1} in SIS-0). Combining these results with ours, the correlation between the continuum flux and O VIII depth becomes clearer. The correlation can be expressed by

$$\tau_{\rm O\,VIII} = (0.38 \pm 0.03)\, C^{-(1.01 \pm 0.21)} \qquad (1)$$

with $\chi^2_\nu = 0.72$ ($\nu = 17$), where C is the count rate and 90% errors are quoted for one interesting parameter. (See figure 2b.) A transient change in the depth of the O VIII edge also occurred in the 1993 July data (Reynolds et al. 1995), similar to the event found here in the 1994 data. Although a recovery of the O VIII depth in the 1994 data is also suggested just after the minimum of the flux at epochs 4 and 12 in our light curve, it is not significant statistically.

3. Discussion

3.1. *Constraints on the Location of the Absorbing Material*

The current observations provide the best constraints yet on the state and location of the warm absorbing

Table 3. Fitting results of the time-divided SIS spectra with a power-law plus two-edge model.

No.	Count rate (c s^{-1} SIS^{-1})	Photon index Γ	N_H ($10^{20}cm^{-2}$)	E_{OVII} (keV)	τ_{OVII}	E_{OVIII} (keV)	τ_{OVIII}	χ^2/d.o.f.
1.....	1.22	$1.95^{+0.07}_{-0.07}$	$0.9^{+1.6}_{-0.9}$	$0.704^{+0.024}_{-0.030}$	$0.56^{+0.16}_{-0.24}$	$0.83^{+0.06}_{-0.07}$	$0.27^{+0.25}_{-0.16}$	457.3/442
2.....	1.62	$1.97^{+0.07}_{-0.06}$	$2.7^{+1.5}_{-1.5}$	$0.722^{+0.016}_{-0.017}$	$0.61^{+0.12}_{-0.13}$	$0.88^{+0.05}_{-0.06}$	$0.19^{+0.11}_{-0.11}$	439.3/467
3.....	1.64	$1.93^{+0.07}_{-0.07}$	$1.9^{+1.8}_{-1.5}$	$0.740^{+0.018}_{-0.034}$	$0.61^{+0.16}_{-0.37}$	$0.90^{+0.17}_{-0.12}$	$0.15^{+0.29}_{-0.10}$	475.1/477
4.....	1.17	$1.88^{+0.09}_{-0.08}$	$1.1^{+2.1}_{-1.1}$	$0.705^{+0.019}_{-0.020}$	$0.62^{+0.18}_{-0.18}$	$0.83^{+0.05}_{-0.03}$	$0.38^{+0.17}_{-0.17}$	394.5/397
5.....	1.60	$2.02^{+0.05}_{-0.06}$	$4.2^{+1.5}_{-1.3}$	$0.724^{+0.016}_{-0.016}$	$0.66^{+0.21}_{-0.16}$	$0.85^{+0.11}_{-0.04}$	$0.30^{+0.16}_{-0.15}$	517.0/497
6.....	1.94	$2.04^{+0.06}_{-0.06}$	$3.7^{+1.3}_{-1.3}$	$0.721^{+0.013}_{-0.015}$	$0.62^{+0.13}_{-0.16}$	$0.85^{+0.07}_{-0.06}$	$0.18^{+0.16}_{-0.11}$	584.5/507
7.....	2.48	$2.05^{+0.05}_{-0.06}$	$4.5^{+1.2}_{-1.2}$	$0.728^{+0.010}_{-0.011}$	$0.77^{+0.11}_{-0.11}$	$0.89^{+0.08}_{-0.04}$	$0.20^{+0.09}_{-0.08}$	502.1/527
8.....	1.78	$1.95^{+0.06}_{-0.05}$	$2.8^{+1.4}_{-1.1}$	$0.719^{+0.016}_{-0.023}$	$0.69^{+0.13}_{-0.20}$	$0.86^{+0.05}_{-0.07}$	$0.22^{+0.19}_{-0.12}$	470.8/502
9.....	1.76	$2.01^{+0.06}_{-0.07}$	$5.2^{+1.6}_{-1.5}$	$0.710^{+0.016}_{-0.016}$	$0.70^{+0.11}_{-0.14}$	$0.90^{+0.05}_{-0.06}$	$0.24^{+0.10}_{-0.09}$	505.0/477
10.....	1.63	$2.05^{+0.06}_{-0.06}$	$5.7^{+1.5}_{-1.2}$	$0.718^{+0.014}_{-0.014}$	$0.68^{+0.14}_{-0.12}$	$0.86^{+0.04}_{-0.04}$	$0.24^{+0.12}_{-0.12}$	529.3/482
11.....	1.43	$2.00^{+0.07}_{-0.06}$	$4.1^{+1.5}_{-1.5}$	$0.722^{+0.016}_{-0.018}$	$0.67^{+0.15}_{-0.21}$	$0.84^{+0.04}_{-0.05}$	$0.24^{+0.18}_{-0.14}$	488.7/482
12.....	1.23	$1.95^{+0.07}_{-0.07}$	$2.4^{+1.6}_{-1.6}$	$0.718^{+0.019}_{-0.019}$	$0.52^{+0.16}_{-0.15}$	$0.85^{+0.03}_{-0.03}$	$0.37^{+0.13}_{-0.14}$	526.6/447
13.....	1.55	$2.02^{+0.08}_{-0.07}$	$3.5^{+1.7}_{-1.6}$	$0.713^{+0.014}_{-0.014}$	$0.67^{+0.12}_{-0.11}$	$0.92^{+0.03}_{-0.04}$	$0.25^{+0.09}_{-0.09}$	416.5/457
14.....	1.39	$1.93^{+0.07}_{-0.07}$	$1.9^{+1.4}_{-1.5}$	$0.718^{+0.017}_{-0.019}$	$0.64^{+0.14}_{-0.17}$	$0.86^{+0.06}_{-0.06}$	$0.21^{+0.14}_{-0.12}$	450.4/457
15.....	1.16	$1.80^{+0.05}_{-0.03}$	$0.0^{+1.4}_{-0.0}$	$0.731^{+0.012}_{-0.013}$	$0.54^{+0.16}_{-0.18}$	$0.86^{+0.05}_{-0.04}$	$0.35^{+0.16}_{-0.15}$	449.0/467
16.....	0.89	$1.87^{+0.04}_{-0.04}$	$0.0^{+0.5}_{-0.0}$	$0.728^{+0.020}_{-0.022}$	$0.64^{+0.14}_{-0.15}$	$0.91^{+0.05}_{-0.04}$	$0.34^{+0.13}_{-0.12}$	423.7/402
17.....	0.65	$1.91^{+0.04}_{-0.05}$	$0.0^{+0.6}_{-0.0}$	$0.716^{+0.020}_{-0.019}$	$0.62^{+0.18}_{-0.16}$	$0.92^{+0.03}_{-0.03}$	$0.63^{+0.14}_{-0.13}$	362.2/341

Note.—The errors are quoted for 90% confidence level for two interesting parameters.

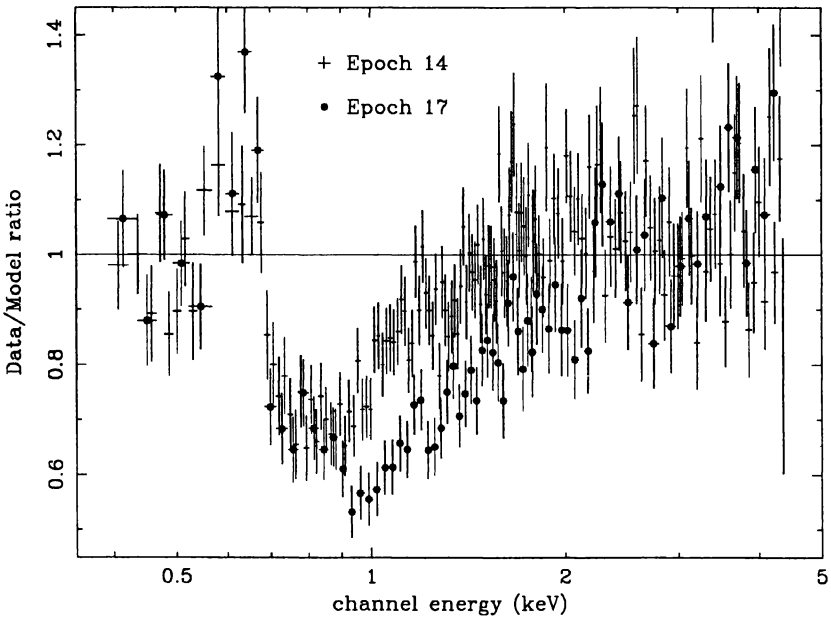

Fig. 3. Comparison of the absorption-edge features at epoch 14 and epoch 17 are shown. The vertical axis shows the ratio from the best-fit power-law determined by the higher and lower energy continua. The difference above 0.9 keV shows the difference of the depth of O VIII absorption edge.

material in this bright Seyfert 1 galaxy. It is clearly seen that the variability of the warm absorber is characterized by a variable O VIII edge and a constant O VII edge. More precisely, the O VII edge appears to be constant over timescales of months to years, whereas the O VIII edge can dramatically increase in optical depth over timescales of 10^4 s or so. The depth of the O VIII edge is anti-correlated with the primary ionizing flux,

thereby providing direct evidence that the material is photoionized.

If the O VII and O VIII edges arise in the same material, (the so-called one-zone models) the recombination and photoionization timescales of these two dominant ions would be comparable. Thus, an unknown mechanism would have to be invoked to stabilize the ionization fraction of O VII whilst allowing the O VIII to respond to the changing ionizing flux. This failure of simple one-zone models prompts us to consider models in which the O VII and O VIII edges originate from spatially distinct regions, one of which is steady and one of which undergoes the observed variations (the two-zone model). Another indication that there are two absorbing regions comes from the possible systematic velocity difference between the two absorption edges discussed in the previous section. Assuming that photoionization controls the ionization state of the warm material, we are led to consider the following model: O VII ions in the region responsible for the O VII edge have a long recombination timescale (i.e., weeks or more), whereas the O VIII edge arises from more highly ionized material (in which most oxygen is fully stripped) in which the O IX ions have a recombination timescale of 10^4 s or less. A decrease in the primary ionizing flux is then accompanied by the recombination of O IX to O VIII, giving the observed variation in the O VIII edge depth. Figure 4 shows the ionization fractions of various states of oxygen as a function of ξ. We postulate that the O VIII absorber exists in the right-hand portion of this figure in which the fraction of O VIII, f_{O8}, is a decreasing function of ξ. In this regime (where oxygen is predominantly in the fully ionized state) $f_{O8} \propto F^{-1}$, where F is the ionizing flux. To see this, note that balancing the photoionization rates with the recombination rates gives

$$f_{O8}\sigma_{O8}F = f_{O9}n_e\alpha, \tag{2}$$

where σ_{O8} is a frequency-weighted mean photoionization cross section for O VIII, and α is the recombination coefficient for O IX. Using $f_{O9} \sim 1$ gives $f_{O8} \propto F^{-1}$. The observed correlation between the O VIII edge depth and the SIS count rate (figure 2b) is in good agreement with this, thereby providing quantitative evidence that photoionization dominates the physics of this plasma.

To observationally characterize the two regions, we select two periods from the long ASCA observation. During the first 300 ks of the observation (which had the primary flux in a high state) the warm absorber was in the low O VIII state; a one-zone photoionization model based on CLOUDY (Ferland 1991, Astronomy Department Internal Report 91-01, Ohio State University) was fitted to this period of data and taken to represent the physical state of the O VII absorber. The best-fit model has a column density of a warm absorber of $N_W = 4.6 \times 10^{21}$ cm^{-2} and an ionization parameter of $\xi = 17.4$ erg cm s^{-1}. In contrast,

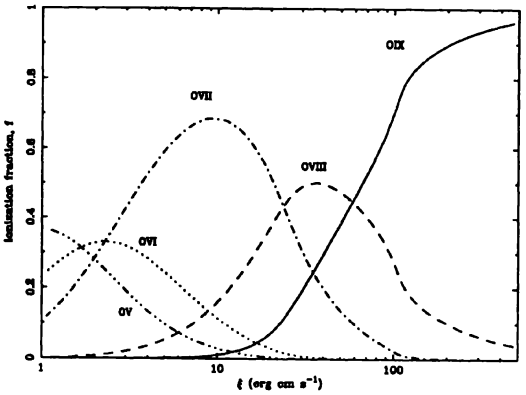

Fig. 4. Ion population of oxygen for the ionization parameter (ξ).

the last 60 ks of the observation (with the primary flux in a low state) had the warm absorber in the high O VIII state. The above parameters for the O VII absorber were held fixed and an additional one-zone model was included to represent the O VIII absorber. This had the parameters $N_W = 1.3 \times 10^{22}$ cm^{-2} and $\xi = 74$ erg cm s^{-1}.

We examined the constraints on each of these regions in the (R, $\Delta R/R$) plane, where R is the distance of the ionized material from the central source of ionizing radiation and ΔR is the line-of-sight distance through the ionized material (which equates to the thickness of a shell in the thin-shell approximation). Physically, $\Delta R/R$ is representative of the volume-filling factor of the material along the line of sight. Using the definition of the ionization parameter,

$$\xi = \frac{L}{N_W R}\frac{\Delta R}{R}, \tag{3}$$

where $N_W = n\Delta R$ is the column density of the ionized material, so that

$$\frac{\Delta R}{R} = \frac{\xi N_W R}{L}. \tag{4}$$

This gives lines A and B in figure 5 for the O VII and O VIII absorbing regions, respectively.

We obtain additional constraints from the recombination timescales of the oxygen ions in the material. The recombination timescale (to all atomic levels) for highly ionized oxygen is given by

$$t_{rec} \approx 200\, n_9^{-1} T_5^{0.7} \text{ s}, \tag{5}$$

where $n = 10^9 n_9$ cm^{-3} and $T = 10^5 T_5$ K is the temperature of the warm material (Shull, van Steenberg 1982). Using the definition of ξ, this can be expressed as

$$t_{rec} \approx 200\, \xi_2 R_{16}^2 L_{43}^{-1} T_5^{0.7} \text{ s}, \tag{6}$$

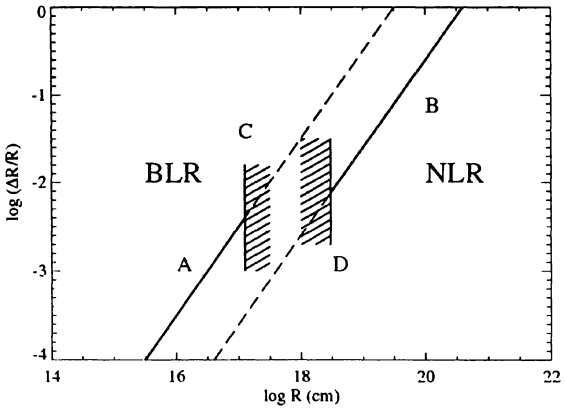

Fig. 5. Constraints in the R–$(\Delta R/R)$ diagram for the inner and outer warm absorbers in the two warm-absorber scheme. Lines A and B show the limits from equation (4) using the determined ξ values in the warm-absorber model. Limits C and D are obtained from equation (6), and the timescales of the column density changes of O VIII and O VII, respectively. The typical distances for BLR and NLR are also indicated.

where $\xi = 10^2\ \xi_2$ erg cm s^{-1}, $R = 10^{16} R_{16}$ cm, and $L = 10^{43} L_{43}$ erg s^{-1}. The ASCA observations require that the O VIII absorber responds on timescales shorter than 10^4 s. We take this to be the limit on the recombination timescale of the O IX ions from which the O VIII ions arise. Thus, assuming $L_{43} = 3$ and utilizing the measured value of ξ for the O VIII absorber gives $R_{16} < 14$ (corresponding to a density limit of $n > 2 \times 10^7$ cm^{-3}). This is limit C in figure 5. Similarly, the constancy of the O VII edge implies a recombination timescale for O VII longer than 10^6 s, which gives $R_{16} > 300$ (corresponding to a density limit of $n < 2 \times 10^5$ cm^{-3}). This is limit D in figure 5.

Recombination to both O VIII and O VII leads to line emission at 0.65 and 0.57 keV, respectively. Since the effective fluorescent yield for this process is about 0.5, significant lines are expected if the warm absorber has a high covering fraction. As already mentioned, since there are large changes in the response function of the SIS near these energies, we must be very cautious in interpreting the observations of such lines. Nevertheless, we do find that the observed flux that can be attributed to line emission is consistent with the above yield, provided that the total covering fraction of the warm absorber is about one half.

3.2. *The Physical Nature of the Warm Material*

The constraints presented above demonstrate that the absorption plausibly occurs in two spatially distinct regions along the line of sight to the primary source. The O VIII absorber is constrained to be at radii characteristic of the broad line region (BLR) with a small volume filling factor ($\Delta R/R < 0.003$) and a density of $n > 2 \times 10^7$ cm^{-3}. Photoionization models give the temperature of this material as $T \sim 10^6$ K, leading to a lower limit on the pressure of $nT > 2 \times 10^{13}$ cm^{-3} K, similar to the pressure of the BLR. It is tempting to identify this with optically-thin clouds in the BLR, which are in approximate pressure balance with the regular broad emission-line clouds.

We note that much of the oxygen in the inner region must be highly ionized (i.e., O IX) and so act as a reservoir for producing O VIII when the flux decreases. The column density of this medium may be $\sim 5 \times 10^{22}$ cm^{-2} and it may be more space filling than the O VIII clouds. Just what its filling factor is can be estimated if it is assumed that the O IX material is heated by radiation and is in pressure equilibrium with the O VIII gas. The temperatures of the O VIII and O IX gas are then about 2×10^5 K and 10^6 K, respectively (see photoionization plots in Reynolds, Fabian 1995). Consequently, the density of the O IX gas is about 5 times smaller than that of the O VIII gas and its volume filling factor is less than 2% (scaling from figure 5). The column density required for the O IX gas to be space filling is thus at least 50 times that of the O VIII absorber, or about 8×10^{23} cm^{-2}. The Thomson depth of such a medium then exceeds 50%, and the variability of the nucleus begins to be smeared out. The above values are taken for the limiting case; more reasonable values lead to the O IX medium being Thomson thick. Such results are contrary to the observed rapid X-ray variability seen in the source (note that electron scattering in the medium would also affect the shape of optical emission line profiles from BLR clouds). We conclude that the O IX reservoir which produces the O VIII absorber is cloudy and pressure-confined by some other medium (or even magnetic fields; Rees 1987) which is yet hotter and less dense.

The O VII absorber is significantly further from the central source and more volume filling ($\Delta R/R > 0.005$). It might be associated with a wind from the putative molecular torus and/or the scattering medium responsible for the scattered continuum in Seyfert 2 galaxies [such as in the models presented by Krolik and Kriss (1995)]. It should be stressed that it is implausible for the O VII edge not to vary unless the associated material is very diffuse (leading to a long recombination timescale). Figure 4 shows that there is no region of parameter space over which the fraction of O VII remains constant when the ionizing flux varies by a few factors. Moreover, models in which an inner O VIII absorbing region shields an outer O VII absorbing region tend to *amplify* the observed variability of the O VII edge. To see this, consider a decrease in flux. Recombination of the O IX ions produces

a deeper O VIII edge which removes photons capable of ionizing O VII. Consequently, the decrease in the ionizing flux at the location of the O VII absorbing region overresponds to the original decrease, thereby producing an over response in the absorption edge. Strictly, this argument is only valid in the regime where f_{O7} decreases with ξ. However, we know that the O VII absorber must exist in this regime due to the absence of an observed O VI edge or indeed oxygen L (and other) absorption (see figure 3).

It is interesting that the column densities of O VII and O VIII ions are comparable. Moreover, the absorption edges in MCG−6–30–15 and many other objects with warm absorbers have maximum optical depths which are on the order of unity. This could be due to the action of radiation pressure on the warm material. Such models require further development.

The authors wish to thank all the ASCA team members whose efforts made this observation and data analysis possible. CO thanks Special Postdoctoral Researchers Program of RIKEN for support. ACF thanks the Royal Society for support. KI thanks the JSPS and the British Council for support.

References

Elvis M., Lockman F.J., Wilkes B.J. 1989, AJ 97, 777
Fabian A.C., Kunieda H., Inoue S., Matsuoka M., Mihara T., Miyamoto S., Otani C., Ricker G. et al. 1994, PASJ 46, L59
Krolik J.H., Kriss G.A. 1995, ApJ 447, 512
Mihara T., Matsuoka M., Mushotzky R.F., Kunieda H., Otani C., Miyamoto S., Yamauchi M. 1994, PASJ 46, L59
Nandra K., Fabian A.C., George I.M., Branduardi-Raymont G., Lawrence A., Mason K.O., McHardy I.M., Pounds K.A. et al. 1993, MNRAS 260, 504
Nandra K., Pounds K.A. 1992, Nature 359, 215
Rees M.J. 1987, MNRAS 228, L47
Reynolds C.S., Fabian A.C. 1995, MNRAS 273, 1167
Reynolds C.S., Fabian A.C., Nandra K., Inoue H., Kunieda H., Iwasawa K. 1995, MNRAS 277, 901
Shull J.M., van Steenberg M. 1982, ApJS 48, 95
Tanaka Y., Nandra K., Fabian A.C., Inoue H., Otani C., Dotani T., Hayashida K., Iwasawa K. et al. 1995, Nature 375, 659